Homooligomerization of the Cytoplasmic Domain of the T Cell Receptor ζ Chain and of Other Proteins Containing the Immunoreceptor Tyrosine-Based Activation Motif†

Alexander Sigalov,* Dikran Aivazian,‡ and Lawrence Stern

Department of Pathology, University of Massachusetts Medical School, 55 Lake Avenue North, Worcester, Massachusetts 01655

Received October 23, 2003; Revised Manuscript Received December 24, 2003

ABSTRACT: Antigen receptors on T cells, B cells, mast cells, and basophils all have cytoplasmic domains containing one or more copies of an immunoreceptor tyrosine-based activation motif (ITAM), tyrosine residues of which are phosphorylated upon receptor engagement in an early and obligatory event in the signaling cascade. How clustering of receptor extracellular domains leads to phosphorylation of cytoplasmic domain ITAMs is not known, and little structural or biochemical information is available for the ITAM-containing cytoplasmic domains. Here we investigate the conformation and oligomeric state of several immune receptor cytoplasmic domains, using purified recombinant proteins and a variety of biophysical and biochemical techniques. We show that all of the cytoplasmic domains of ITAM-containing signaling subunits studied are oligomeric in solution, namely, T cell antigen receptor ζ, CD3ε, CD3δ, and CD3γ, B cell antigen receptor Igα and Igβ, and Fc receptor FcεRIγ. For ζ_{cyt}, the oligomerization behavior is best described by a two-step monomer−dimer−tetramer fast dynamic equilibrium with dissociation constants in the order of ∼10 μM (monomer−dimer) and ∼1 mM (dimer−tetramer). In contrast to the other ITAM-containing proteins, $Ig\alpha_{cyt}$ forms stable dimers and tetramers even below 10 μM. Circular dichroic analysis reveals the lack of stable ordered structure of the cytoplasmic domains studied, and oligomerization does not change the random-coil-like conformation observed. The random-coil nature of ζ_{cyt} was also confirmed by heteronuclear NMR. Phosphorylation of ζ_{cyt} and $Fc\epsilon RI\gamma_{cyt}$ does not significantly alter their oligomerization behavior. The implications of these results for transmembrane signaling and cellular activation by immune receptors are discussed.

Antigen recognition by immune cells resulting in the initiation of various immune responses is mediated by the interaction of membrane-bound receptors with soluble, particulate, and cellular antigens. The basis for this transmembrane signal transduction mechanism is not fully understood but is thought to depend on receptor clustering and/or conformational changes, which then trigger an intracellular tyrosine phosphorylation cascade (*1*, *2*). The family of antigen receptors named multichain immune recognition receptors (MIRR) (*3*) shares common structural and functional features, including multiple subunits having a single transmembrane (TM) span, with extracellular ligand-binding domains and intracellular signaling domains carried on separate subunits. Members of this family include the T cell receptor (TCR)[1] complex, the B cell receptor (BCR) complex, the type 1 receptor for IgE (FcεRI), and the high- and low-affinity receptors for IgG, FcγRI (CD64) and FcγRIII (CD16). It has been suggested that MIRR employ similar downstream signal transduction mechanisms involving members of the src family of protein tyrosine kinases, which are activated by antigen−receptor interaction and which couple antigen binding to downstream signal transduction processes (*4*, *5*).

The general architecture of the BCR and TCR complexes is similar (*6*). Each has antigen-binding units (mIg and TCRαβ, respectively) with single transmembrane spans per subunit and small intracellular tails. The antigen-binding subunit(s) of each receptor associate(s) noncovalently with heterodimeric signaling components (Igαβ in the BCR, CD3δε, and CD3γε in the TCR) that have single Ig-family extracellular domains, single transmembrane spans, and apparently unstructured intracellular domains of 40−60 residues. The TCR has an additional component, the ζ homodimer. Each ζ subunit has a small extracellular region (9 residues) carrying the intersubunit disulfide bond, a single

† This study was funded by the National Science Foundation (NSF; project MCB-0091072).

* Corresponding author. Phone: 508-856-8803. Fax: 508-856-0019. E-mail: Alexander.Sigalov@umassmed.edu.

‡ Present address: Department of Biochemistry, Stanford University, Stanford, CA 94305.

[1] Abbreviations: BCR, B cell receptor; BS^3, bis(sulfosuccinimidyl) suberate; CD, circular dichroism; DMS, dimethyl suberimidate; DTT, 1,4-dithiothreitol; ES-MS, electrospray mass spectrometry; GF, gel filtration; GdnHCl, guanidine hydrochloride; HSQC, heteronuclear single-quantum correlation; ITAM, immunoreceptor tyrosine-based activation motif; MALDI-MS, matrix-assisted laser desorption ionization mass spectrometry; MHC, major histocompatibility complex; NMR, nuclear magnetic resonance; PBS, phosphate-buffered saline (1 mM KH_2PO_4, 10 mM Na_2HPO_4, 137 mM NaCl, 2.7 mM KCl); RP-HPLC, reverse-phase high-performance liquid chromatography; SDS−PAGE, sodium dodecyl sulfate−polyacrylamide gel electrophoresis; TCR, T cell receptor; TFA, trifluoroacetic acid.

10.1021/bi035900h CCC: $27.50
Published on Web 01/30/2004

transmembrane span per subunit, and a large, apparently unstructured cytoplasmic domain of ~110 residues. The TCR ζ subunit can occasionally be substituted by an alternately spliced version (η). The high-affinity type 1 receptor for IgE (FcϵRI) has a related structure, with an mIg-like Fc-binding subunit (FcϵRIα), a multipass transmembrane subunit (FcϵRIβ), and a ζ-like signaling subunit (FcϵRIγ). TCRζ and FcϵRIγ are functionally interchangeable in some systems (*7*). For TCR and BCR, assembly of the various ligand-binding and signaling units is believed to be mediated by interactions within the transmembrane domains (*8*).

A common feature of the members of the MIRR family is the presence of one or more copies of a cytoplasmic structural module termed the immunoreceptor tyrosine-based activation motif (ITAM) (*9*). ITAMs consist of conserved sequences of amino acids that contain two appropriately spaced tyrosines (YxxL/Ix_{6-8}YxxL/I, where x denotes non-conserved residues) (*9*). Following receptor engagement, phosphorylation of ITAM tyrosine residues by src family kinases represents one of the earliest events in the signaling cascade (*10*, *11*). Among the TCR-associated chains, ζ is particularly interesting due to the presence of three ITAMs in its cytoplasmic tail, allowing for multiple phosphorylation states (*12*, *13*). In general, phosphorylation of both tyrosines within an ITAM is thought to be essential for signaling, as this is required for efficient recruitment of the tandem SH2 domain containing protein kinases Syk and ZAP-70 to the receptor complex (*14*, *15*). The syk-family kinases are activated by binding to phosphorylated ITAM domains carried on the receptor domains, and their activation results in recruitment of adapter and effector proteins such as LAT, SLP-76, and PKCΘ, which couple receptor engagement to downstream signaling pathways, leading eventually to activation of transcription factors such as NF-κB, NF-AT, and AP-1 (*16*).

The mechanism of transmembrane signal transduction by these receptors is poorly understood. Receptor clustering, rather than ligand binding per se, is thought by most workers in the field to be critical for activation (*17*−*25*). The dependence of activation on ligand valency has been studied in detail for the TCR, BCR, and FcϵRI (*17*, *24*−*31*). In each case, binding of multivalent but not monovalent ligand is thought to be required to trigger activation processes. However, some reports have suggested that monovalent ligand binding can trigger clustering, and ligand-induced intrareceptor conformational changes recently have been suggested by several researchers (*18*, *32*−*34*).

Crystal structures are available for the extracellular ligand-binding domains of the TCR and FcϵRI in the absence and presence of ligand (*35*−*39*). For both receptors, only relatively small conformational changes and loop rearrangements not likely to be coupled to transmembrane signaling events were observed upon ligand binding. Little structural or biochemical information is available for the ITAM-containing cytoplasmic domains. It is assumed that these cytoplasmic domains are mostly random-coil polypeptides in solution (*40*−*42*).

How clustering of the extracellular domains of MIRR leads to activation and phosphorylation of their cytoplasmic domain ITAMs is not clear. It is known that dynamic changes in oligomeric state can play an important role in transducing signals from the cell surface to the nucleus in many systems (*43*). There is also a body of evidence that a highly flexible, random-coil-like conformation is the native and functional state under physiological conditions for many proteins to be involved in cell signaling and regulation (*44*, *45*). The number of intrinsically disordered proteins known to be functional in oligomerization or protein−protein binding is growing rapidly (*44*−*48*).

Despite the important role of ITAM-containing cytoplasmic domains in cellular signaling systems, the specific oligomeric state of these proteins has not been investigated. In the present study, we examined the conformation and oligomeric state of several immune receptor cytoplasmic domains, using purified recombinant proteins and a variety of biophysical and biochemical techniques. The proteins studied were overproduced and purified from *Escherichia coli*. Using a combination of gel filtration, dynamic light scattering, analytical ultracentrifugation, and chemical cross-linking methods, we demonstrated that homooligomerization under physiological conditions is a common feature of the ITAM-containing cytoplasmic domains of the TCR- and BCR-associated signal transduction subunits and of the FcϵRI receptor γ chain. For ζ_{cyt}, circular dichroic analysis revealed a random-coil-like conformation for both monomeric and oligomeric forms, as confirmed by two-dimensional heteronuclear NMR spectroscopy. Phosphorylation of ζ_{cyt} and FcϵRIγ_{cyt} did not significantly alter their oligomerization behavior. We also found that Igα_{cyt} forms tightly bound homodimers and higher homooligomers (mostly, tetramers) even at low protein concentrations at which the other ITAM-containing cytoplasmic domains studied were monomeric.

EXPERIMENTAL PROCEDURES

Reagents. Bovine thrombin (catalog no. 154163, 2430 units/mg) was purchased from ICN Biomedicals (Costa Mesa, CA). Bis(sulfosuccinimidyl) suberate was obtained from Pierce Biotechnology (Rockford, IL). Dithiothreitol and urea were purchased from Sigma Chemical Co. (St. Louis, MO). Ni-NTA−agarose was procured from Qiagen (Valencia, CA). All other chemicals used were of high quality analytical grade. All solutions were made in Milli-Q water.

Cloning, Expression, and Purification. The cDNAs for the cytoplasmic domains of the human ITAM-containing proteins (CD3ϵ, 57 AA, P07766, SwissProt; CD3δ, 46 AA, P04234; CD3γ, 46 AA, P09693; TCRζ, 115 AA, P20963; TCR-Cys-ζ, 118 AA, see below; FcϵRIγ, 44 AA, P30273; Igα, 63 AA, P11912; and Igβ, 51 AA, P40259) were cloned into the pET32a(+) vector (Novagen) downstream of the thioredoxin (Trx) and His_6 tag coding sequences. The original enterokinase site, which has proven to be inadequate for this application, has been replaced by a thrombin site in all of the proteins. The constructions were designed so that, after cleavage, the recombinant proteins each begin with GS followed by the native sequence. The plasmid used to express ζ_{cyt} protein begins with a five-residue sequence carrying the unique Cys residue (Cys-ζ_{cyt}) used to form the $\zeta_{cyt}-\zeta_{cyt}$ dimer (MKKCGLRVKFSR...LPPR) and was kindly provided by Dr. Winfried Weissenhorn (EMBL, Grenoble, France). The expression plasmids were transformed into the BL21(DE3) strain of *E. coli*.

The following general procedure was used for protein expression and purification. A single colony was inoculated

into 100 mL of LB broth containing 50 μg/mL ampicillin and grown at 37 °C for 16 h. The cells were inoculated into 1 L of LB medium containing 50 μg/mL ampicillin, grown to an OD_{600} value of 0.9−1.2, and induced with 0.4 mM isopropyl β-D-thiogalactopyranoside. After 3 h, the cells were harvested, and the pellet was resuspended in 100 mL of the lysis buffer (10 mM Tris, 100 mM NaH_2PO_4, pH 8.0) containing 8 M urea. The cell suspension was stirred at 4 °C for 16 h. It was then centrifuged at 6500*g* for 15 min, and the supernatant was directly loaded onto a Ni-NTA−agarose column preequilibrated with the same buffer. The column was washed with the lysis buffer (pH 8.0), and the protein eluted using the same buffer with gradual pH reduction according to the manufacturer's instructions. The fractions containing the target fusion protein were pooled, subjected to dialysis against 14 L of 20 mM HEPES (pH 7.5) containing 150 mM NaCl and 0.1 mM DTT for 16 h at 4 °C with two changes, and centrifuged at 6500*g* for 15 min. Then, the protein was digested at 25 °C for 1 h in the presence of 1 mM DTT and 5 mM $CaCl_2$ with 6 units of thrombin/mg of protein to remove the N-terminal His_6-tagged thioredoxin. The digest was quenched by addition of PMSF to a final concentration of 0.1 mg/mL and diluted 2-fold with 0.1% TFA. Then, a reverse-phase HPLC separation was performed on a C18 Vydac 22 × 250 mm preparative column (Vydac, Hesperia, CA) with a linear acetonitrile gradient (0−72%) with 0.1% TFA (12 mL/min). The fractions containing the target protein were identified by Tricine SDS−PAGE (12.5%), pooled, and lyophilized.

For ζ_{cyt} protein purification, an additional ion-exchange chromatographic step was added to the general purification scheme. After digestion with thrombin, the digest was quenched by addition of PMSF to a final concentration of 0.1 mg/mL, diluted 5-fold with 20 mM NaH_2PO_4 (pH 6.0), and loaded on a column (10 × 250 mm) packed with a strong cation exchanger POROS 20 HS (Applied Biosystems, Foster City, CA) and preequilibrated with the same buffer. Proteins were eluted with a 140 mL linear NaCl gradient (from 0 to 360 mM) at a rate of 8 mL/min. Fractions containing ζ_{cyt} protein were pooled, diluted 2-fold with 0.1% TFA, and subjected to a preparative reverse-phase HPLC separation as described above. The ζ_{cyt} protein was unstable at low pH (<5) due to cleavage of the Asp93−Pro94 amide bond, as confirmed by analytical RP-HPLC, mass spectroscopy, and N-terminal sequencing (results not shown).

The purity and identity of the proteins obtained were confirmed by Coomassie-stained Tricine SDS−PAGE (12.5%), analytical RP-HPLC, ES-MS, and N-terminal sequencing.

Oxidation of Cys-Containing ζ_{cyt}. Disulfide-linked ζ_{cyt} was obtained by air oxidation in the presence of 1 mM $CuSO_4$ and 3.9 mM *o*-phenanthroline as previously described (*49*). Briefly, Cys-ζ_{cyt} was incubated with 5 mM freshly prepared DTT at 4 °C for 16 h with following dialysis against 3 L of 20 mM HEPES (pH 7.7) at 4 °C for 16 h with two changes. Then, *o*-phenanthroline (ethanol solution, 65 mM) and 25 mM $CuSO_4$ were added to final concentrations of 3.9 and 1.0 mM, respectively. The reaction mixture was incubated at 20 °C for 16 h with following dialysis against 3 L of 20 mM HEPES (pH 7.7) at 20 °C for 24 h with three changes. It was centrifuged at 6500*g* for 15 min and subjected to RP-HPLC using a C4 Vydac 10 × 250 mm semipreparative column (Vydac, Hesperia, CA) with a linear acetonitrile gradient (0−50%) with 0.1% TFA (12 mL/min). Purity and identity of the obtained $\zeta_{cyt}-\zeta_{cyt}$ dimer were confirmed by Tricine SDS−PAGE (12.5%), ES-MS, and analytical RP-HPLC.

Gel Filtration Chromatography. Analytical HPLC gel filtration of purified proteins was performed at ambient temperature using a Phenomenex BioSep-SEC-S2000 column (7.8 mm × 300 mm). After the column was equilibrated with elution buffer PBS (pH 7.0), 20 μL protein samples were injected and separated at a flow rate of 0.6 mL/min. Elution was monitored by recording the absorbance at 214 and 280 nm. Protein concentrations ranged from 2 to 800 μM. Flow rate, sample volume, the absolute protein amount injected, and pH values of an elution buffer were varied in some subsets of gel filtration experiments as indicated in the Results section. For calibration, the following molecular mass markers (Bio-Rad Laboratories, Hercules, CA) were used: bovine thyroglobulin (670 kDa), bovine γ-globulin (158 kDa), chicken ovalbumin (44 kDa), horse myoglobulin (17 kDa), and vitamin B_{12} (1.35 kDa). The data, apparent molecular mass versus loading protein concentration, were analyzed using the softwares KaleidaGraph (version 3.51; Synergy Software, Reading, PA) and CurveExpert (version 1.36; Daniel Hyams). The final model was chosen, and the relevant dissociation constants were calculated from the best fit analysis of the data to each of the following models: monomer−dimer, monomer−trimer, monomer−tetramer, monomer−dimer−trimer, and monomer−dimer−tetramer association.

Light Scattering. Scattering data were collected at 20 °C (or in the 5−50 °C temperature range as indicated in the Results section) with a DynaPro-MS800 instrument (Protein Solutions, Charlottesville, VA). Protein solutions were prepared in a PBS buffer (pH 7.4) and filtered with 0.22 μm Millex filters prior to measurements. Final protein concentrations ranged from 7.6 to 760 μM. During the illumination, the photons scattered by proteins were collected at 90° on 1−5 s acquisition times (depending on a protein concentration). In dynamic light scattering experiments, translational diffusion coefficients (D) were determined from scattering data with the DYNAMICS autocorrelation analysis software (version 5.25.44; Protein Solutions). D is converted to a hydrodynamics radius R_h through the Stokes−Einstein equation ($R_h = kT/6\pi\eta D$, where η is the solvent viscosity, k is the Boltzmann constant, and T is the temperature) and then to a molecular mass using a coil model. Concentration dependence data obtained in dynamic experiments, apparent molecular mass versus protein concentration, were analyzed using the same software and fitting models as described above. As indicated in the Results section, in some subsets of dynamic light scattering experiments the protein samples were prepared in the presence of 5 M GdnHCl and incubated for 16 h at 4 °C before the measurements were taken.

In static light scattering experiments, the Debye analysis (*50*) was applied to calculate the molecular masses of the protein species from their scattering intensity over that of the solvent using toluene as a scattering standard. The change in the refractive index of protein solutions as a function of protein concentration (increment of refractive index, dn/dc) was assumed to be similar to that of most proteins and was taken as 0.20 mL/g.

Cross-Linking. Protein samples were incubated for 8−24 h at 20 °C in 10 mM sodium phosphate, pH 8.3 (with or without 150 mM NaCl, unless mentioned otherwise), in the presence of BS^3 (or DMS or glutaraldehyde in some subsets of cross-linking experiments). Final protein concentrations ranged from 4 to 380 μM, and final concentrations of the cross-linking reagent varied from 0.2 to 20 mM as indicated in the Results section. Cross-linked samples were boiled for 5 min with SDS sample buffer (4% SDS, 3% β-mercaptoethanol, 0.01% bromophenol blue). Regular or Tricine SDS−PAGE was carried on 12.5% gels. For calibration, the BenchMark prestained protein ladder (Invitrogen, Carlsbad, CA) molecular mass markers were used. After being run, gels were scanned, and the gel images were analyzed using ImageJ (version 1.26t; NIH, Bethesda, MD) and KaleidaGraph (version 3.51, Synergy Software, Reading, PA) to calculate an apparent molecular mass and the relative amount of protein species.

Circular Dichroism Measurements. Far-UV CD spectra were recorded on an Aviv 202 spectropolarimeter (AVIV Instruments, Lakewood, NJ) with 0.01 and 1.0 mM ζ_{cyt} protein in PBS (pH 7.0) in 1.0 and 0.01 mm path-length cells, respectively. Data were collected at 25 °C every nanometer from 260 to 190 nm with 1.0 s averaging per point and a 1 nm bandwidth. The CD spectra of at least six scans were signal averaged, baseline corrected by subtracting an averaged buffer spectrum, and normalized to molar residue ellipticity.

Mass Spectrometry. Protein samples were applied onto a MALDI target in 50% ACN/0.1% TFA/matrix (α-cyano-4-hydroxycinnamic acid)/water, and the molecular masses were determined using a Voyager Elite STR (Perseptive Biosystems, Cambridge, MA) mass spectrometer. ES-MS was performed at the Department of Chemistry Instrumentation Facility (Massachusetts Institute of Technology, Cambridge, MA) using a Bruker Daltonics APEX II 3 Tesla Fourier transform mass spectrometer supplied with an electrospray ionization source (Bruker Daltonics, Inc., Billerica, MA).

Analysis of Phosphorylation Pattern. Phosphorylation of ζ_{cyt} and FcϵRIγ_{cyt} in a final protein concentration of 0.01 or 0.2 mM was performed at 37 °C using a recombinant protein tyrosine kinase *src*(86−536) (0.2 μM) in 20 mM HEPES (pH 7.5) containing 150 mM NaCl, 2 mM MgATP, 10 mM $MgCl_2$, and 50 μM Na_3VO_4 as described (*40*). The phosphorylation patterns at 0.5, 1, 2, and 4 h of incubation were analyzed using Tricine SDS−PAGE (12.5%) with subsequent gel scanning and analyzing as described above. The extent of phosphorylation in phospho-ζ_{cyt} (4 and 6 mol of phosphate/mol of protein, respectively) and phospho-FcϵRIγ_{cyt} (1 and 2 mol of phosphate/mol of protein, respectively) was determined by MALDI-MS of the relevant protein species purified using reverse-phase HPLC. Purified completely phosphorylated ζ_{cyt} and FcϵRIγ_{cyt} (6 and 2 mol of phosphate/mol of protein, respectively) were further used for gel filtration, cross-linking, and dynamic light scattering experiments.

Analytical Ultracentrifugation. Sedimentation equilibrium experiments of ζ_{cyt} were performed in PBS (pH 7.4) at 20 °C in a Beckman Optima XL-A analytical ultracentrifuge equipped with absorbance optics and a four-hole An60Ti rotor with standard 1.2 cm hexasector cells. Samples were run at five different speeds (12000, 15000, 18000, 21000, and 24000 rpm) for six different loading protein concentrations (0.1, 0.3, 0.5, 0.76, 0.88, and 0.99 mM). Data were acquired at 280 and 292 nm over a 30 h period as averages of 10 measurements of absorbance data in the step scan mode, with a radial step size of 0.003 cm. Blank runs, used to make optical background corrections, were performed under the same conditions. Data sets were collected after reaching equilibrium, as judged by the absence of systematic deviations between successive scans taken 2 h apart after the initial ~20 h equilibration. After data at equilibrium had been collected, the rotor speed was increased to 45000 rpm to deplete the meniscus. This procedure allowed the baseline at the meniscus to be measured experimentally.

To estimate monomeric molecular mass and the self-association constant(s), the Optima XL-A data analysis software package was used to perform a global nonlinear regression of the data obtained from the three centrifuge cells at various rotor speeds. The behavior of ζ_{cyt} protein under a given set of conditions (three loading protein concentrations of 0.3, 0.5, and 0.99 mM at three different rotor speeds of 15000, 18000, and 21000 rpm) was chosen for detailed analysis. A partial specific volume of 0.7168 $cm^3\ g^{-1}$ at 20 °C for ζ_{cyt} protein was estimated from amino acid composition using the Sednterp software (version 1.06; University of New Hampshire). The solvent density was set to 1.005. Dissociation constants were calculated from the best fit analysis of the data to each of the following models: ideal nonassociating monomer, monomer−dimer, monomer−trimer, monomer−tetramer, monomer−dimer−trimer, and monomer−dimer−tetramer association. The association constants obtained from self-association models were converted to a molar scale using the calculated molar extinction coefficient of the protein. The final model was chosen so that (a) the estimated monomeric molecular mass was closest to that predicted from the amino acid sequence, (b) the value for the "goodness of fit", defined as $\sum$(residual/standard error)^2/(degrees of freedom), was the smallest, and (c) the distribution of error was random about a zero mean (*51*).

NMR Spectroscopy. For NMR spectroscopy, uniformly ^{15}N-labeled ζ_{cyt} protein was expressed in 10 L of minimal medium containing KH_2PO_4 (1.6 g/L), Na_2HPO_4 (10 g/L), sodium citrate (1 g/L), $MgSO_4$ (0.24 mg/L), thiamin (10 mg/L), $(NH_4)_2SO_4$ (0.7 g/L), ampicillin (50 μg/mL), and trace metals, supplemented with glucose and [^{15}N]ammonium sulfate as sole carbon and nitrogen sources, respectively. The ^{15}N-labeled protein was purified according to the protocol described above and kept at 0.9 mM in 20 mM sodium phosphate buffer (pH 6.2, with or without 100 mM NaCl) and 90% H_2O/10% D_2O. All $^1H-^{15}N$ HSQC experiments (*52*) were performed at the Center for Magnetic Resonance (Massachusetts Institute of Technology, Cambridge, MA) on a custom-built spectrometer CMR600E, operating at 600 MHz and recorded at 20 °C using a triple resonance probe. The carrier frequency was set at the center of the spectrum at the water frequency. The data were processed by using the program FELIX (Molecular Simulations, San Diego, CA) to a final matrix size of 1024 × 1024.

RESULTS

Expression and Purification of Cytoplasmic Domains of ITAM-Containing Proteins. The cytoplasmic domains of T

Table 1: Molecular Mass of ζ_{cyt}[a]

calcd MW (Da)	ES-MS MW (Da)	gel filtration MW (kDa)	light scattering MW (kDa)		analytical ultracentrifugation MW (kDa)
			static	dynamic	
13157	13157	27.1 (±1.5)	28.3 (±2.7)	25.4 (±2.4) 13.2 (±1.8)[b]	26.0 (±1.3)

[a] The calculated molecular mass was derived from the protein sequence. Molecular mass was experimentally determined by electrospray mass spectrometry (ES-MS), gel filtration, static and dynamic light scattering, and analytical ultracentrifugation as described in the Experimental Procedures section. Values in parentheses are the standard errors. Sedimentation equilibrium data assume that standard errors for each data point are equal to the square root of the χ^2 values. [b] In the presence of 5 M GdnHCl.

cell receptor subunits CD3ϵ, CD3δ, CD3γ, and ζ, B cell receptor subunits Igα and Igβ, and the Fcϵ receptor γ subunit were expressed in *E. coli* as soluble His_6-tagged thioredoxin fusion proteins. Typically, a 1 L culture contained a wet cell mass of 4.5−5.0 g, which yielded 10−12 mg of a recombinant ITAM-containing protein, free of the N-terminal His_6 tag and thioredoxin fusion partner, and purified to ≥96% homogeneity as verified by Tricine SDS−PAGE overloaded with up to 20 μg of protein per lane. For expression and purification of ζ_{cyt} (both unlabeled and uniformly ^{15}N-labeled), a larger volume of culture was used (10 L), and an additional ion-exchange chromatographic step was added to provide ≥99% homogeneity (Tricine SDS−PAGE), giving a final yield of protein of about 80 mg. Cys-ζ_{cyt}, used to prepare the disulfide-linked $\zeta_{cyt}-\zeta_{cyt}$ dimer, was expressed in *E. coli* as a soluble polypeptide, isolated, and oxidized essentially as described (*49*).

The ζ_{cyt} Is Predominantly Dimeric, and the Oligomerization Is Reversible and Dependent on Concentration and Temperature. The apparent molecular mass of ζ_{cyt} was determined using gel filtration, sedimentation equilibrium, and light scattering (Table 1). As compared to the molecular mass predicted from the sequence and confirmed by mass spectroscopy (13157 Da), the native apparent molecular mass indicated the formation of oligomeric forms, with the predominant species a dimer in rapid equilibrium with monomer and larger oligomers. These results are described in detail below.

(1) Gel Filtration Analysis. Gel filtration chromatography is widely used for determination of the size and molecular mass of proteins under native conditions, and it is a useful technique to monitor molecular association/dissociation. Gel filtration chromatography was performed for ζ_{cyt} and a range of molecular mass markers using a Phenomenex BioSep-SEC-S2000 column. As shown in Figure 1A, ζ_{cyt} (500 μM loading concentration) had a retention volume of 8.1 mL, between that of chicken ovalbumin (7.5 mL, 44 kDa) and horse myoglobulin (8.6 mL, 17 kDa). A calibration curve fit to the molecular mass standards (Figure 1A, broken line) was used to determine the apparent native molecular mass for ζ_{cyt} as 27.1 ± 1.5 kDa (mean ± SD), consistent with that of a ζ_{cyt} dimer. At least three independent experiments were performed for this determination. For comparison, we also investigated the gel filtration behavior of the disulfide-linked ($\zeta_{cyt}-\zeta_{cyt}$) dimer on the same column. Since the sequences of both ζ_{cyt} and Cys-ζ_{cyt} are almost identical, the apparent molecular mass of covalently bound dimer (at low protein concentration) should correspond to that obtained for ζ_{cyt}, if the latter protein is predominantly dimeric. The apparent native molecular mass of $\zeta_{cyt}-\zeta_{cyt}$ (0.3 mg/mL) as determined by gel filtration was ~27 kDa (data not shown), as expected for the covalent dimer and consistent with the molecular mass observed by ES-MS and predicted by the protein sequence (27118 Da). This strongly supports the valid application of the gel filtration chromatography in this study.

To characterize the equilibrium between monomeric and oligomeric forms of ζ_{cyt} in solution, we performed gel filtration experiments using various protein loading concentrations ranging from 0.02 to 10 mg/mL. As the loading concentration was decreased, the retention volume of ζ_{cyt} shifted from the value corresponding to dimer to that of monomer (Figure 1B). These data were fit to all of the models described in the Experimental Procedures section. The best fit, as judged by smaller standard error and larger correlation coefficient, was given by the two-step monomer−dimer−tetramer equilibrium model (Figure 1C, solid line). The analysis estimated the apparent monomer−dimer and the dimer−tetramer equilibrium dissociation constants, $K_{d(monomer-dimer)}$ and $K_{d(dimer-tetramer)}$, as 9.2 ± 1.6 μM and 0.9 ± 0.2 mM (mean ± a standard deviation), respectively. Computational analysis (*53*) using these values predicts that ζ_{cyt} is predominantly dimeric in solution for concentrations between 10^{-4} and 10^{-6} M.

We performed several tests to rule out artifactual explanations for the apparent oligomerization behavior. The reproducibility of the molecular mass marker retention times analyzed before and after each analytical series indicates that the shift was not related to possible systematic error caused by instrumental instability. To evaluate the potential effect of protein−matrix interactions and dilution factor on the ζ_{cyt} retention volume, in some subsets of gel filtration experiments the injected sample volume was kept constant (20 μL) and the total protein amount in the samples was varied from 0.5 to 200 μg (2−760 μM), while in other experiments the injected volume of was varied from 3 to 600 μL keeping a constant total protein amount (~15 μg). No significant difference in concentration dependence of retention volume was observed in either set of experiments. The self-association of ζ_{cyt} is readily reversible since nearly identical concentration dependence curves were obtained regardless of whether samples were prepared by serial dilutions of the 600 μM protein sample or by initial dissolution of the lyophilized protein to the desired concentrations. The apparent oligomerization behavior was independent of flow rate (from 0.5 to 0.9 mL/min) and pH value of an elution buffer (from 6.0 to 8.0). The observed gradual shift of retention volume with increasing protein concentration, rather than an appearance of new peaks and a change in the intensity of peaks corresponding to ζ_{cyt} monomer and oligomer, may indicate a fast dynamic equilibrium between monomeric and oligomeric ζ_{cyt} species (see below).

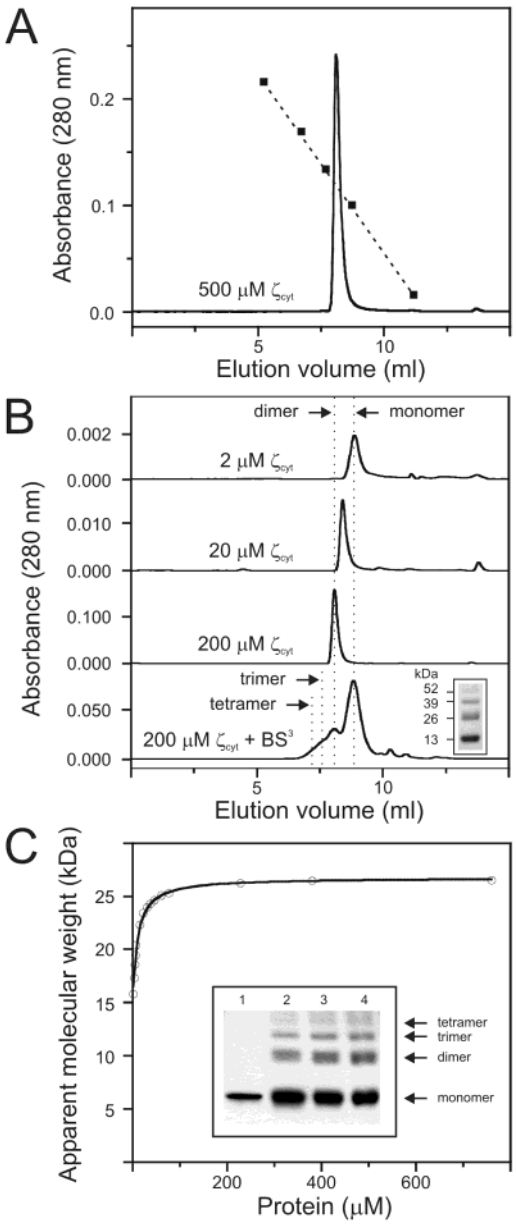

FIGURE 1: Gel filtration analysis of the oligomeric state of ζ_{cyt}. (A) Phenomenex BioSep-SEC-S2000 (7.8 mm × 300 mm) gel filtration chromatography of ζ_{cyt} (30 μL, 500 μM loading protein concentration) as indicated by the solid line. The apparent molecular mass of ζ_{cyt} (27 kDa) was determined on the basis of the relationship of the elution volumes of markers versus their molecular masses. The fitted calibration curve is indicated by a broken line showing log MW plotted against the elution volume of molecular mass markers (bovine thyroglobulin, 670; bovine γ-globulin, 158; chicken ovalbumin, 44; horse myoglobulin, 17; and vitamin B_{12}, 1.35 kDa) marked by filled squares. (B) Typical gel filtration profiles of ζ_{cyt} with loading protein concentrations of 2, 20, and 200 μM. Gel filtration and SDS−PAGE (inset) profiles of BS^3 cross-linked ζ_{cyt} are also shown. Broken lines indicate calculated elution volumes of monomeric, dimeric, trimeric, and tetrameric forms of ζ_{cyt} based on molecular mass markers. (C) Concentration dependence of the apparent molecular mass of ζ_{cyt} (open circles) as studied by gel filtration at 20 °C. The data were fit to monomer−dimer−tetramer (ζ_{cyt}) and monomer−dimer (ζ_{cyt}−ζ_{cyt}) equilibrium models (solid line). The inset shows the SDS−PAGE (12.5%) profiles of non-cross-linked (lane 1) and BS^3 cross-linked ζ_{cyt} of 0.5, 1.0, and 2.5 mg/mL (lanes 2, 3, and 4, respectively). The apparent molecular masses of monomeric and oligomeric ζ_{cyt} were calculated, and the relevant bands were identified on the basis of the relationship of the electrophoretic mobilities of markers versus their molecular masses.

(2) Cross-Linking Studies. Chemical cross-linking studies were carried out to further characterize the oligomeric state of ζ_{cyt} in solution. Neither glutaraldehyde nor dimethyl suberimidate cross-linking resulted in detectable amounts of ζ_{cyt} oligomers, as analyzed by SDS−PAGE, but bis(sulfosuccinimidyl) suberate (BS^3) cross-linking (Figure 1C, inset) resulted in monomeric (~13 kDa), dimeric (~26 kDa), trimeric (~39 kDa), and tetrameric (~52 kDa) species. The total amount of oligomeric species observed increased with increasing protein concentration, and the relative amounts of oligomeric species were dependent on protein concentration, in a manner consistent with a concentration-dependent oligomerization process. Varying NaCl concentration from 0 to 150 mM, or BS^3 concentration from 0.2 to 20 mM, did not result in any significant differences in relative amounts of ζ_{cyt} oligomers (data not shown).

Considering that the cross-linking experiment should trap the oligomers that are normally in a dynamic equilibrium with the monomers, gel filtration analysis of the BS^3 cross-linked 200 μM ζ_{cyt} sample was performed at the same conditions as for the non-cross-linked protein (Figure 1B, bottom trace). In contrast to the gel filtration profile of non-cross-linked ζ_{cyt} at the same loading protein concentration, the profile of cross-linked ζ_{cyt} exhibited separated peaks, with retention volumes corresponding to those of the monomeric and dimeric forms. Small amounts of trimeric and tetrameric forms were also apparent. The relative amounts of monomeric (68%) and oligomeric (32%) forms of ζ_{cyt} as determined by gel filtration were nearly identical to those obtained by SDS−PAGE (64% and 36%, respectively). Most of the cross-linked ζ_{cyt} remains as a monomer, suggesting that the degree of cross-linking obtained in this experiment disrupts the noncovalent self-association of this protein, due to the steric constraints resulting from intramolecular cross-link formation and/or chemical modification of the residues involved in protein−protein interactions. The difference in gel filtration patterns for non-cross-linked and cross-linked ζ_{cyt} supports the existence of a fast dynamic equilibrium between monomeric and oligomeric ζ_{cyt} species in solution.

(3) Analytical Ultracentrifugation. Sedimentation equilibrium analytical ultracentrifugation allows direct determination of absolute molecular mass, independent of shape. Using this technique, it is possible to determine both the stoichiometry and equilibrium constants for the species present. To distinguish between multiple species arising either from a rapidly reversible association or from the presence of irreversible aggregates, the data obtained at different cell loading concentrations and rotor speeds should be examined.

To further investigate the oligomerization state of ζ_{cyt}, sedimentation equilibrium experiments were performed with the purified protein (Figure 2). The data obtained at PBS, pH 7.4, and 20 °C were fit to all of the models described in the Experimental Procedures section. Fitting with a single species model, the apparent weight-average molecular mass of the system was ~26 kDa (Table 1), suggesting that ζ_{cyt} self-associates. For fitting with models describing self-association, the molecular mass of monomeric ζ_{cyt} was initially fixed to the value calculated from the amino acid sequence (13157 Da) and allowed to float after fits to other parameters had converged. Floating the molecular mass resulted in less than a 1% change in its value. The best fit,

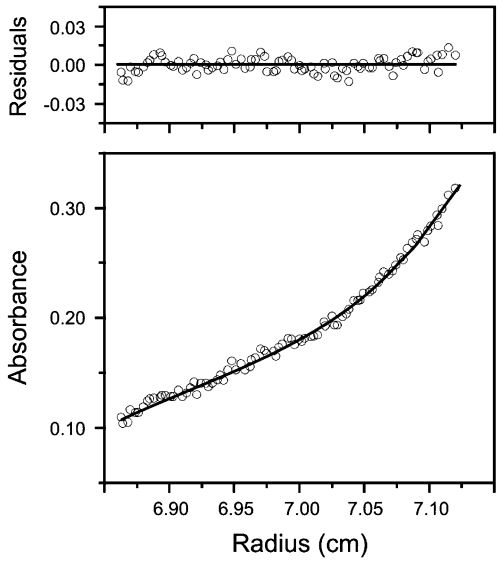

FIGURE 2: Sedimentation equilibrium analysis of the oligomeric state of ζ_{cyt}. Panels show plots of absorbance (bottom panel) and residuals (upper panel). Open circles show the UV absorbance gradient in the centrifuge cell (500 μM loading protein concentration). The data were fit to a monomer−dimer−tetramer equilibrium model, and the solid line denotes the fitted curve calculated from three speeds and multiple protein concentrations. Residuals show the difference in the fitted and experimental values as a function of radial position.

as judged by (1) estimated monomeric molecular mass closest to that predicted from the amino acid sequence and confirmed by ES-MS, (2) the lowest goodness-of-fit value, and (3) random distribution of residuals, was obtained with a model for reversible monomer−dimer−tetramer equilibrium (Figure 2, solid line). For the calculation of the dissociation constants (K_d) of ζ_{cyt}, monomeric molecular mass of 13157 Da (Table 1) and molar extinction coefficient of 9.10 $mM^{-1}cm^{-1}$ were used. The analysis estimated the monomer−dimer and the monomer−tetramer equilibrium dissociation constants, $K_{d(monomer-dimer)}$ and $K_{d(monomer-tetramer)}$, respectively. From that the dimer−tetramer dissociation constant, $K_{d(dimer-tetramer)}$, was obtained by the relation $K_{d(monomer-tetramer)}/(K_{d(monomer-dimer)})^2$ (*51*). For the model used, $K_{d(monomer-dimer)}$ and $K_{d(dimer-tetramer)}$ were 12.1 ± 3.3 μM and 1.1 ± 0.3 mM (mean ± SD), respectively.

Thus, the apparent molecular mass and dissociation constants determined using sedimentation equilibrium analytical ultracentrifugation are in agreement with gel filtration data and indicate that ζ_{cyt} is predominantly dimeric in solution.

(4) Dynamic and Static Light Scattering. Light scattering is a rapid and nondestructive method to measure the hydrodynamic properties of proteins as they freely diffuse in solution. In static light scattering (SLS) experiments, the concentration-dependent scattering intensity of the sample solution is used to determine the absolute molecular mass of the analyte under examination. The apparent molecular mass of ζ_{cyt} was characterized with static light scattering. Extrapolated to infinite dilution, the apparent molecular mass was 28.3 ± 2.7 kDa (mean ± SD), consistent with that of a ζ_{cyt} dimer (Table 1).

In dynamic light scattering (DLS) experiments, the size distribution and the translational diffusion coefficient D of a protein can be measured without calibration. The apparent

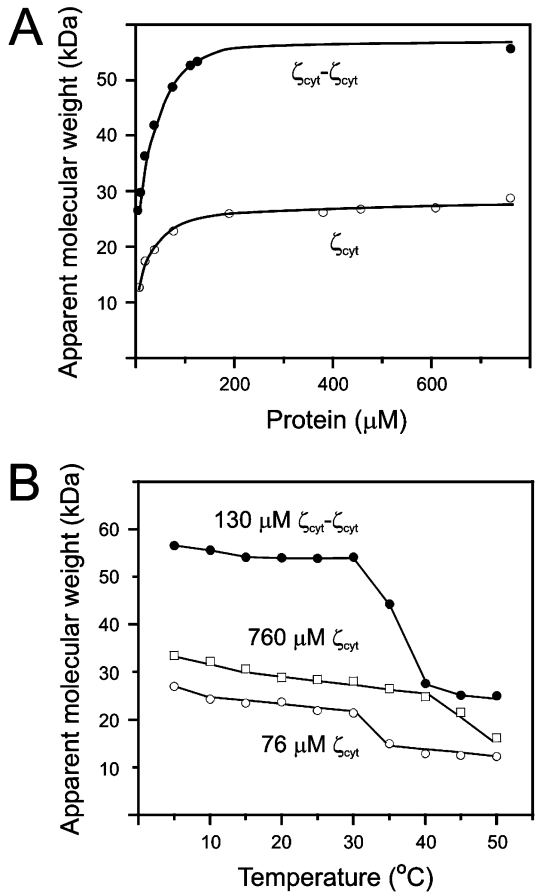

FIGURE 3: Concentration and temperature dependence of the apparent molecular mass of ζ_{cyt} monitored by dynamic light scattering. (A) Concentration dependence of the apparent molecular mass of ζ_{cyt} (open circles) and of $\zeta_{cyt}-\zeta_{cyt}$ (filled circles). For $\zeta_{cyt}-\zeta_{cyt}$, we use the term monomer−dimer equilibrium model to describe the equilibrium between monomeric and dimeric forms of the covalently bound dimer. (B) Temperature dependence of the apparent molecular mass of ζ_{cyt} (760 and 76 μM; open squares and circles, respectively) and $\zeta_{cyt}-\zeta_{cyt}$ (130 μM; filled circles), as determined by dynamic light scattering at the indicated temperatures. Lines connecting the data points are shown.

molecular mass estimated from dynamic light scattering for ζ_{cyt} at 20 °C is plotted as a function of protein concentration in Figure 3A (open circles). For comparison, the concentration dependence of the apparent molecular mass of the disulfide-linked $\zeta_{cyt}-\zeta_{cyt}$ dimer is also indicated (Figure 3A, closed circles). The molecular masses for both ζ_{cyt} (25.4 ± 2.4 kDa) and disulfide-linked $\zeta_{cyt}-\zeta_{cyt}$ (53.4 ± 5.2 kDa) are about 2 times the relevant monomeric molecular masses of 13157 and 27118 Da, respectively. As a control, we investigated ζ_{cyt} in the presence of GdnHCl, which at high concentration should disrupt noncovalent interactions mediating oligomerization. Addition of 5 M GdnHCl to 200 μM ζ_{cyt} solution in PBS results in a reduction of ζ_{cyt} apparent molecular mass to 13.2 ± 1.8 kDa (mean ± SD; Table 1), similar to that of the ζ_{cyt} monomer observed at low concentration. These findings indicate that ζ_{cyt} and $\zeta_{cyt}-\zeta_{cyt}$ most likely exist as dimers in solution under the conditions studied (for $\zeta_{cyt}-\zeta_{cyt}$, the dimeric form contains two copies of the covalently bound dimer). As described above for data from gel filtration, we fit the concentration dependence of the apparent molecular mass of ζ_{cyt} and $\zeta_{cyt}-\zeta_{cyt}$ to various oligomerization models. For ζ_{cyt}, data from dynamic light

scattering experiments were best fit to the monomer−dimer−tetramer equilibrium model (Figure 3A) with $K_{d(monomer-dimer)}$ and $K_{d(dimer-tetramer)}$ of 38.2 ± 19.6 μM and 1.5 ± 0.6 mM (mean ± SD), respectively. The best fit for the disulfide-linked $\zeta_{cyt}-\zeta_{cyt}$ was given by the monomer−dimer equilibrium model (Figure 3A) with $K_{d(monomer-dimer)}$ of 28 ± 9.4 μM (mean ± SD).

The temperature dependence of the apparent molecular mass as determined by dynamic light scattering was measured for ζ_{cyt} and $\zeta_{cyt}-\zeta_{cyt}$ (Figure 3B). For ζ_{cyt} at 76 μM (open circles), the apparent molecular mass changed from ~25 kDa at lower temperatures to ~12 kDa at higher temperatures, with the transition occurring between 30 and 40 °C. A similar shift was also found for $\zeta_{cyt}-\zeta_{cyt}$ (130 μM, filled circles), where the apparent molecular mass changed from ~55 to ~25 kDa with increasing temperature. The temperature-induced transition range for ζ_{cyt} was concentration-dependent, tending to higher temperature values with increasing protein concentration. At 760 μM (open squares), the transition range starts at ~40 °C, approximately 10 °C higher than for ζ_{cyt} at 76 μM (open circles). All proteins remained soluble under all conditions studied, and the temperature-induced dimer dissociation was reversible for both ζ_{cyt} concentrations, as shown by decreasing temperature from 50 to 5 °C, which resulted in reversal of the temperature-induced changes (data not shown).

In summary, solution studies by light scattering indicate that ζ_{cyt} is monomeric below 10 μM. At higher concentrations oligomers (mostly dimers) are formed, the equilibrium between these forms being dependent on temperature and the ζ_{cyt} concentration. This behavior is consistent with gel filtration and sedimentation equilibrium experiments. Dissociation constants values determined by this method are also in line with those determined by gel filtration analysis and analytical ultracentrifugation.

ζ_{cyt} Is an Unstructured, Random-Coil Protein, and Its Oligomerization Does Not Result in Formation of Detectable Secondary or Tertiary Structure. (1) CD Spectroscopy. The far-ultraviolet CD spectra of ζ_{cyt} show the characteristics of an unfolded protein (Figure 4A), consistent with earlier published results (*40*, *49*). Spectra obtained at 0.01 and 1 mM concentration, at which ζ_{cyt} is mostly monomeric and dimeric, respectively, were essentially superimposable (solid and dotted lines). The spectra did not change significantly with changes in ionic strength (0−0.2 M NaCl; data not shown). No changes were observed in the CD spectrum when ζ_{cyt} was completely phosphorylated (data not shown). Considering that the CD spectra for both protein concentrations are similar, it can be concluded that oligomerization does not lead to formation of secondary or tertiary structure.

(2) NMR Spectroscopy. In recent years NMR spectroscopy has become uniquely useful in characterization of the structure and dynamics of unfolded and partially folded proteins (*46*, *47*, *54*−*57*). The $^1H-^{15}N$ HSQC spectrum of 0.87 mM ζ_{cyt} was acquired at 15 °C to further confirm the unfolded state of the protein inferred from CD spectroscopy. Essentially all of the cross-peaks expected for a 115 amino acid residue protein were observed (112) in the spectrum of ζ_{cyt}. As shown in Figure 4B, the spectrum presents features resembling that of an unfolded state, particularly with the backbone amide ^1H chemical shifts spanning only 7.6−8.6 ppm (1.0 ppm). This low dispersion of the backbone amide

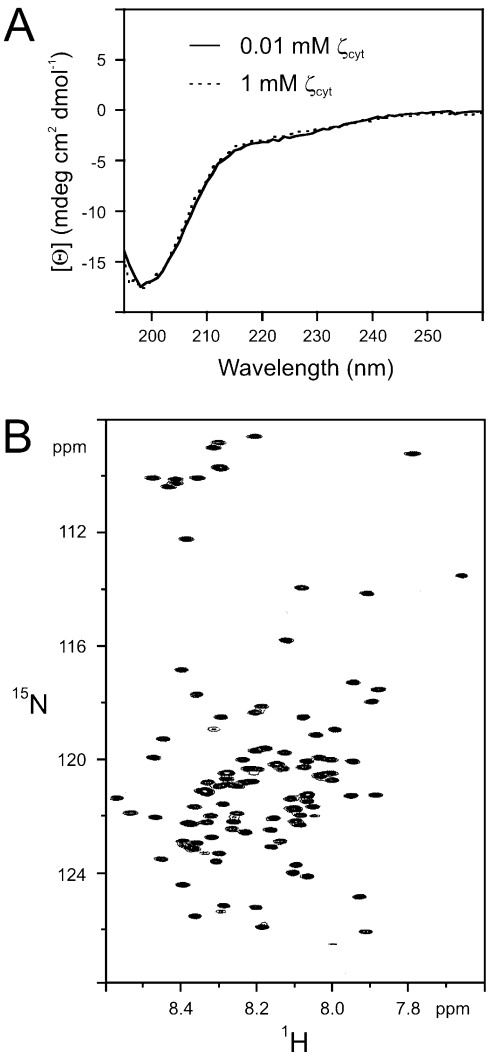

FIGURE 4: Secondary structure of ζ_{cyt} as studied by circular dichroism and NMR spectroscopy. (A) Far-ultraviolet CD spectra of ζ_{cyt}. The mean residue ellipticity is plotted as a function of wavelength for 0.01 (solid line) and 1 mM ζ_{cyt} (broken line) in PBS (pH 7.0) in 1.0 and 0.01 mm path-length cells, respectively. (B) $^1H-^{15}N$ HSQC spectrum of 0.87 mM uniformly ^{15}N-labeled ζ_{cyt} recorded at 15 °C.

^1H chemical shifts is typical for unfolded or intrinsically disordered proteins (*54*, *55*, *57*). The dispersion of backbone amide ^{15}N shifts in the unfolded state of proteins is not as dramatically reduced relative to the folded state. The dispersion of ^{15}N shifts (20 ppm) observed for ζ_{cyt} is well consistent with those published for other unfolded or intrinsically disordered proteins (*54*, *55*, *57*).

Thus, according to both CD and NMR spectroscopy, oligomerization of ζ_{cyt} does not induce detectable secondary or tertiary structure.

Homooligomerization Is a Common Structural Feature of Cytoplasmic Domains of ITAM-Containing Proteins. To investigate the oligomeric state of cytoplasmic domains of the other ITAM-containing proteins, we experimentally determined the apparent molecular masses of CD3ϵ_{cyt}, CD3δ_{cyt}, CD3γ_{cyt}, FcϵRIγ_{cyt}, Igα_{cyt}, and Igβ_{cyt}. As compared to the molecular mass values predicted from the sequences and confirmed by mass spectroscopy, the native apparent molecular masses determined using gel filtration and dynamic light scattering suggest the formation of predominantly

Table 2: Molecular Masses of Cytoplasmic Domains of Other ITAM-Containing Proteins Studied[a]

protein	calcd MW (Da)	ES-MS MW (Da)	gel filtration MW (kDa)	dynamic light scattering MW (kDa) no GdnHCl	dynamic light scattering MW (kDa) 5 M GdnHCl
CD3ϵ_{cyt}	6323	6325	12.5 (±1.4)	11.9 (±2.2)	7.6 (±1.8)
CD3δ_{cyt}	5140	5140	8.6 (±1.2)	9.4 (±2.1)	5.6 (±0.8)
CD3γ_{cyt}	5370	5372	11.8 (±1.4)	10.8 (±2.4)	6.1 (±1.0)
FcϵRIγ_{cyt}	5010	5010	11.1 (±1.4)	9.6 (±1.4)	4.6 (±0.5)
phospho-FcϵRIγ_{cyt}	5186	5182	12.1 (±1.6)	10.5 (±1.6)	5.3 (±0.6)
Igα_{cyt}[b]	7142	7142	18.3 (±2.0) 37.4 (±3.1)	19.7 (±2.8)	8.5 (±1.9)
Igβ_{cyt}	5654	5654	12.3 (±1.4)	10.2 (±2.3)	5.0 (±0.7)

[a] The calculated molecular masses were derived from protein sequences. Molecular masses were experimentally determined by electrospray mass spectrometry (ES-MS), gel filtration, and dynamic light scattering as described in the Experimental Procedures section. Values in parentheses are the standard errors. [b] The values determined for dimeric and tetrameric Igα_{cyt} are indicated.

dimeric species for each of these proteins above 0.1 mM (Table 2). Addition of GdnHCl resulted in dissociation of oligomers, with apparent molecular mass values determined by DLS in the presence of 5 M GdnHCl close to those measured by mass spectroscopy and corresponding to monomers (Table 2). The observed GdnHCl-induced oligomer dissociation was reversible, and removal of GdnHCl by dialysis resulted in increasing of apparent molecular mass values to those corresponding to dimers (data not shown).

For studying the equilibrium between monomeric and oligomeric forms of ITAM-containing proteins in solution, we performed gel filtration experiments with multiple protein loading concentrations. For CD3ϵ_{cyt}, CD3δ_{cyt}, CD3γ_{cyt}, FcϵRIγ_{cyt}, and Igβ_{cyt} (but not Igα_{cyt}; see below), the gel filtration patterns and the concentration dependence of retention times and therefore of apparent molecular mass values were similar to those observed for ζ_{cyt} (data not indicated). The gel filtration data indicated that there exists a fast dynamic equilibrium between monomeric and dimeric cytoplasmic domains of all of the ITAM-containing proteins studied, again with the exception of Igα_{cyt} (see below). The self-association of these proteins is readily reversible since nearly identical concentration dependence curves were obtained regardless of whether samples were prepared by dilution of concentrated stock solutions or by initial dissolution of the lyophilized proteins to the desired concentrations.

In contrast to the other ITAM-containing proteins studied, two well-separated peaks were observed by gel filtration for Igα_{cyt} with apparent molecular masses corresponding to monomeric and dimeric species at low protein concentration (Figure 5A) and to tetrameric and dimeric species at high protein concentration (Figure 5B). Even below 10 μM, where the other ITAM-containing proteins were mostly monomeric, Igα_{cyt} was mostly dimeric. The amount of tetrameric form increased with increasing protein loading concentration, and this equilibrium was slowly reversible (data not shown). The peaks corresponding to tetrameric and dimeric Igα_{cyt} were isolated and reinjected onto the same column (Figure 5, panels C and D, respectively). No differences in retention time values were observed for these peaks. These results suggest that for Igα_{cyt} the dynamic equilibrium between

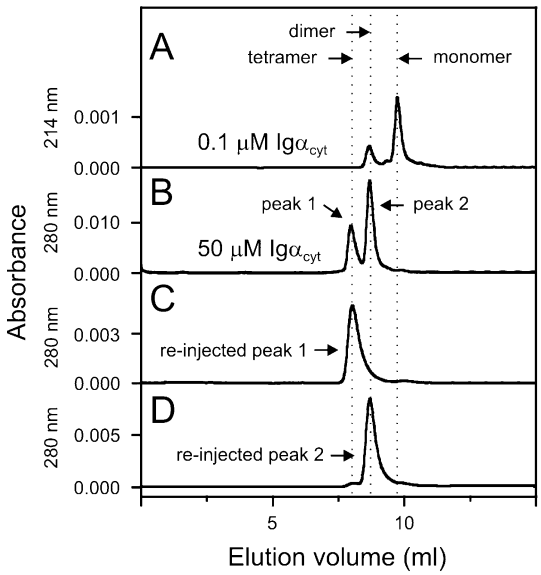

FIGURE 5: Gel filtration analysis of the oligomeric state of Igα_{cyt}. Gel filtration profiles of Igα_{cyt} with loading protein concentrations of 0.1 and 50 μM (panels A and B, respectively). Broken lines indicate calculated elution volumes of monomeric, dimeric, and tetrameric forms of Igα_{cyt} based on molecular mass markers. When analyzing the 50 μM Igα_{cyt} sample, peaks 1 and 2 were collected manually and reinjected onto the same column (panels C and D, respectively).

monomeric and oligomeric species is slower and the protein−protein interaction is stronger than those observed for other proteins studied. In the Igα/Igβ/mIg B cell receptor complex, Igα tends to bind more readily to src family members than does Igβ (*58*), and it activates tyrosine kinases more efficiently (*59*, *60*). It remains unclear if this feature of Igα may be attributed to the unique ability of its cytoplasmic domain to form, in solution, stable homooligomers (mostly, dimers and tetramers) even at very low protein concentrations where Igβ_{cyt} and other cytoplasmic domains of ITAM-containing proteins studied are mostly monomeric.

To further investigate the oligomeric state of the cytoplasmic domains of the ITAM-containing proteins in solution, chemical cross-linking studies were carried out at 20 °C in 10 mM sodium phosphate and 150 mM NaCl (pH 8.3), using BS^3 as a cross-linking agent. SDS−PAGE analysis of the cross-linked proteins revealed the presence of oligomeric species for all of the proteins (Figure 6). Again, Igα_{cyt} exhibited a greater tendency toward tetramerization than the other proteins. Additional cross-linking experiments (not shown) also indicated that relative amounts of oligomeric species are dependent on protein concentration and that a total amount of these species increases with increasing protein concentration in the reaction mixture (data not shown). The results of the cross-linking experiments therefore support the oligomeric state for the cytoplasmic domains of the ITAM-containing proteins studied.

CD analysis of CD3ϵ_{cyt}, CD3δ_{cyt}, CD3γ_{cyt}, FcϵRIγ_{cyt}, Igα_{cyt}, and Igβ_{cyt} showed that these proteins are unstructured, random-coiled proteins. In each case, no detectable secondary or tertiary structure was observed with increasing protein concentration (data not shown). Thus, as for ζ_{cyt}, the cytoplasmic domains of other ITAM-containing proteins appear to be unstructured in both monomeric and oligomeric states.

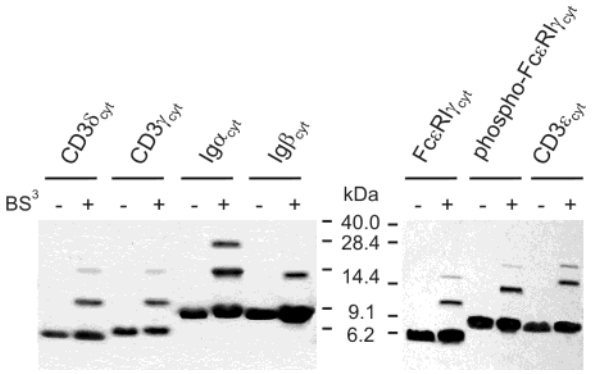

FIGURE 6: Oligomeric state of ITAM-containing cytoplasmic domains as studied by chemical cross-linking. Tricine SDS−PAGE (12.5%) profiles of the 0.15 mM un-cross-linked (odd lanes) and BS^3 cross-linked (even lanes) cytoplasmic domains of ITAM-containing proteins are shown. The apparent molecular masses of monomeric and oligomeric forms were calculated, and the relevant bands were identified on the basis of the relationship of the electrophoretic mobilities of markers versus their molecular masses (positions of the molecular mass markers bands are indicated).

Oligomerization of ζ_{cyt} Does Not Block the Phosphorylation of the ITAM Tyr Residue, and Completely Phosphorylated ζ_{cyt} Is Predominantly Dimeric in Solution. ζ_{cyt} can be efficiently phosphorylated in vitro by recombinant protein tyrosine kinases *lck* or *src*, as shown previously (*40*, *49*). In this study, when phosphorylation of ζ_{cyt} is analyzed using a soluble version of *src* (containing residues 86−536) (*61*), complete reaction at either high (0.2 mM) or low (0.01 mM) ζ_{cyt} concentration, where the protein predominantly is dimeric or monomeric, respectively, resulted in 6 mol of phosphate incorporated/mol of protein (data not shown). Similarly, for FcϵRIγ_{cyt}, reaction with *src*(86−536) at both high and low FcϵRIγ_{cyt} concentrations resulted in complete phosphorylation (2 mol of phosphate/mol of protein). These data are consistent with the results of another study (*62*) where the kinase *lck* was used for complete phosphorylation of the ζ_{cyt} ITAM tyrosines at a ζ_{cyt} concentration (84 μM) where, according to the results presented here, the protein is predominantly dimeric. These results suggest that oligomerization does not block the phosphorylation of any of the ITAM Tyr residues of either ζ_{cyt} or FcϵRIγ_{cyt}.

Gel filtration, cross-linking, and dynamic light scattering studies of phospho-ζ_{cyt} and phospho-FcϵRIγ_{cyt} showed that both proteins form oligomers in solution, again with dimers as the predominant species at concentrations above 0.1 mM (data not shown). For phospho-ζ_{cyt}, addition of 5 M GdnHCl results in reduction of apparent molecular mass from 28.0 ± 2.8 to 14.1 ± 1.6 kDa (mean ± SD), as determined by DLS. This value is similar to those of the phospho-ζ_{cyt} monomer observed at low concentration or calculated from protein sequence (13580 Da). Similar GdnHCl-induced dimer dissociation was observed for phospho-FcϵRIγ_{cyt} (Table 2). In both cases, this dissociation can be reversed by removal of GdnHCl using dialysis or gel filtration. In summary, monomers and oligomers in rapid equilibrium coexist in solution below 0.1 mM for both phospho-ζ_{cyt} and phospho-FcϵRIγ_{cyt}, as they do for the corresponding unphosphorylated forms.

DISCUSSION

The ability of cytoplasmic domains of ITAM-containing proteins to adopt multimeric structures was assessed by gel filtration, sedimentation equilibrium ultracentrifugation, light scattering, and cross-linking studies. We have demonstrated, for the first time, that ζ_{cyt} as well as the cytoplasmic domains of other ITAM-containing proteins studied, namely, CD3ϵ_{cyt}, CD3δ_{cyt}, CD3γ_{cyt}, FcϵRIγ_{cyt}, Igα_{cyt}, and Igβ_{cyt}, is predominantly dimeric in solution but can also form higher oligomers. Interestingly, our dynamic light scattering data on ζ_{cyt} (Table 1) are consistent with those reported earlier for this protein (*40*), where an average molecular mass of 25 ± 3 kDa was determined using this technique, but this higher value as compared to that for monomer (14 kDa) was attributed by the authors to a nonglobular shape for monomeric ζ_{cyt} (*40*). We have shown also that completely phosphorylated ζ_{cyt} and FcϵRIγ_{cyt} (6 and 2 mol of phosphate/mol of protein, respectively) are dimeric in solution. Thus, all of the cytoplasmic domains of ITAM-containing proteins studied form noncovalently linked dimers and higher oligomers, which are in a concentration- and temperature-dependent equilibrium with monomers.

According to a two-step monomer−dimer−tetramer equilibrium model, the dissociation constants for ζ_{cyt} are in the order of ~10 μM and ~1 mM for the monomer−dimer and dimer−tetramer equilibria, respectively. Formation of oligomers higher than dimer may indicate that the dimer interface between two ζ_{cyt} monomers involves nonidentical surfaces, such that each monomer in a dimer retains a second surface that is available for further oligomerization. While this association is relatively weak, particularly for the higher order oligomers, the associated extracellular and transmembrane domains may substantially strengthen oligomerization of the whole protein molecule and stabilize the oligomers formed. For example, the extracellular domain of CD3ϵ has been found to be able to form homooligomers, and the same 16 amino acid region has been suggested to be the major contributor to the formation of homo- and heterodimers among the CD3ϵ, CD3γ, and CD3δ chains (*63*). Furthermore, as recently shown using experimental, computational, and evolutionary approaches (*64*, *65*), the transmembrane domain of ζ in its native state (a lipid bilayer) may be present in a tetrameric form, and so homooligomerization of ζ may be driven in vivo not only by its cytoplasmic tail but also by its transmembrane domain.

It is possible that oligomerization of receptor cytoplasmic domains potentially might result in reduced accessibility to other components of the cellular signaling machinery. This phenomenon does not appear to be active here, as both ζ_{cyt} and FcϵRIγ_{cyt} can be efficiently phosphorylated in vitro under conditions were they are present predominantly as oligomers. Moreover, cellular studies have shown that ζ_{cyt} and Igα_{cyt}, oligomerized intracellularly by cell-permeable chemical inducers of dimerization, retain the ability to be phosphorylated and to initiate cytoplasmic signaling cascades (*66*, *67*). These data suggest that should self-association of the cytoplasmic domains of ζ and other ITAM-containing proteins occur in vivo, it would not block phosphorylation of ITAM Tyr residues.

Dimerization/oligomerization as a general control mechanism in signal transduction has been widely discussed (*43*,

68), and the physiological relevance of oligomerization of cytoplasmic domains of different receptors has been extensively studied during the last years. For example, it has been shown that homooligomerization of the erythropoietin receptor (EPOR) cytoplasmic tail is involved in the formation and activation of the EPOR signal transduction complex (*69*). Homooligomerization of integrins driven by both transmembrane and cytoplasmic domains has also been reported recently (*70*), and it was suggested that this homomeric interaction might contribute to the clustering of integrins that accompanies cellular adhesion. These particular proteins are characterized by a well-defined three-dimensional structure. In contrast, as we show in this study, the cytoplasmic domains of ζ and other ITAM-containing proteins are mostly unfolded proteins in a random-coil-like conformation. Such unfolded domains are increasingly recognized as potentially important players in signaling processes. A computational analysis of intrinsic disorder tendencies has shown that a larger number of signaling proteins from the database of the Alliance for Cellular Signaling have predicted disordered regions of >30 consecutive residues, as compared to typical eukaryotic proteins from the SWISS-PROT database, and that these differences rise with increasing numbers of consecutive residues in predicted disordered regions (*44*). The lack of folded structure in signaling proteins might give these proteins a functional advantage over globular proteins with well-defined secondary and tertiary structure: the ability to bind to multiple different targets without sacrificing specificity. In addition, binding of intrinsically disordered proteins to their interacting partners (other proteins, ligands, lipids, etc.) often is accompanied by induction and stabilization of secondary structure. Indeed, we have previously shown that binding of ζ_{cyt} to acidic lipids induces formation of helical structure (*49*). Also, it has been shown recently that TCR engagement causes a change in CD3ε that allows accessibility to Nck, an adaptor protein thought to play an important role in T cell signaling (*32*, *33*). The homooligomerization of the cytoplasmic domains of ζ and other ITAM-containing proteins observed here might play an important role in T and B cell signaling by assisting in conformation changes that release the relevant cytoplasmic domains in ready-to-get phosphorylated forms, or by assisting in formation of signaling scaffolds that bring together receptor cytoplasmic domains, protein kinases, and various adapter/effector proteins, into a correct orientation and in sufficient proximity in the receptor cluster/oligomer to create a competent, activated receptor complex.

The TCR ζ chain contains a single cysteine residue, located in the highly conserved but very short extracellular domain of the protein, which in vivo is found as a disulfide bond covalently linking the ζ homodimer. TCR signaling efficacy is dramatically reduced for ζ mutants in which the disulfide bond has been shifted by one or more residues, while a mutant ζ chain obtained by replacing the cysteine with a glycine and therefore having no disulfide bond functionally behaves indistinguishably from the wild-type protein (*71*). These results highlight the importance of orientation effects within an ζ oligomer and indicate that the precise arrangement of cytoplasmic domains within an oligomer could be linked to their ability to interact with cytoplasmic signaling machinery. Since substitution of the ζ extracellular cysteine does not abrogate homodimer formation (*71*), interactions elsewhere in the protein must contribute to homodimer stability. While it has been suggested that the ζ chain transmembrane domain contributes to stabilization of the homodimer (*72*), the oligomerization behavior shown here for ζ_{cyt} indicates that the cytoplasmic domain may play an important role as well.

T cell receptor complexes on resting cells include TCRαβ, CD3δε, CD3γε, and ζζ components. After stimulation of cells through the TCR, there is physical dissociation of the receptor complex, such that the CD3 and ζ chains dissociate independently from the remaining receptor subunits (*73*−*75*). The ability of the cytoplasmic tails of ζ and CD3 subunits to oligomerize, as observed in the present study, may provide some driving force for this structural reorganization of the TCR complex upon T cell triggering. Following clustering of receptor extracellular domains, homooligomerization of the cytoplasmic domains could result in formation of multimeric species such as $CD3(\delta\epsilon\epsilon\gamma)_2$ and $(\zeta\zeta)_2$ and therefore assist in dissociation of CD3 and/or ζ from the TCR complex. Similar mechanisms also may be involved in the rapid turnover of the ζ chain in resting T cells, which has been shown to be independent from the rest of the TCR−CD3 complex (*76*). Antigenic stimulation of the BCR has been reported recently also to result in physical dissociation of the receptor complex, with Igα/Igβ signaling subunits dissociating from mIg (*77*). As suggested above for CD3 and ζ chains, homooligomerization of $Ig\alpha_{cyt}$ and $Ig\beta_{cyt}$ described in this study might be one of the mechanisms involved in BCR structural reorganization upon binding to self or foreign antigen. Finally, the mast cell/basophil high-affinity IgE receptor (FcεRI) also has been shown recently to dissociate upon antigenic stimulation, with distinct aggregation of FcεRIβ and FcεRIγ subunits after activation (*78*). The intrinsic tendency of the FcεRIγ cytoplasmic domain to form oligomers in solution may play a role in the activation-induced dissociation of FcεRI or subsequent cellular events, as suggested above also for TCR and BCR.

In summary, our data suggest that there is an interesting rule which may shed more light on the function and physiological role of ITAM-containing receptor signaling subunits: their cytoplasmic domains form homooligomers in solution and are very likely to be a new class of intrinsically disordered protein domains. Since this oligomerization does not block phosphorylation of the ITAM Tyr residues, it can be also suggested that formation of the cytoplasmic domain oligomers of the ITAM-containing receptor signaling subunits may contribute to receptor clustering/oligomerization and cellular activation. Further structural and/or mutagenesis studies are needed to determine which amino acid residues are involved in this interaction and whether there exists a specific oligomerization motif in these protein domains. We are presently investigating these possibilities.

ACKNOWLEDGMENT

We thank Mia Rushe for excellent technical assistance. Special thanks to Dr. Thomas Cameron for helpful advice and discussions during the course of these studies and for important comments on the manuscript. Dr. Christopher Turner and the Harvard University/Massachusetts Institute of Technology Center for Magnetic Resonance are thanked for NMR experiments. Jennifer Stone is thanked for constant support and helpful discussions.

SUPPORTING INFORMATION AVAILABLE

Results of curve fitting of gel filtration, dynamic light scattering, and sedimentation equilibrium data to various oligomerization models. This material is available free of charge via the Internet at http://pubs.acs.org.

REFERENCES

1. Van der Merwe, P. A., Davis, S. J., Shaw, A. S., and Dustin, M. L. (2000) Cytoskeletal polarization and redistribution of cell-surface molecules during T cell antigen recognition, *Semin. Immunol. 12*, 5−21.
2. Van der Merwe, P. A. (2001) The TCR triggering puzzle, *Immunity 14*, 665−668.
3. Keegan, A. D., and Paul, W. E. (1992) Multichain immune recognition receptors: similarities in structure and signaling pathways, *Immunol. Today 13*, 63−68.
4. Cambier, J. C., and Jensen, W. A. (1994) The hetero-oligomeric antigen receptor complex and its coupling to cytoplasmic effectors, *Curr. Opin. Genet. Dev. 4*, 55−63.
5. Birkeland, M. L., and Monroe, J. G. (1997) Biochemistry of antigen receptor signaling in mature and developing B lymphocytes, *Crit. Rev. Immunol. 17*, 353−385.
6. Cambier, J. C. (1992) Signal transduction by T- and B-cell antigen receptors: converging structures and concepts, *Curr. Opin. Immunol. 4*, 257−264.
7. Krishnan, S., Warke, V. G., Nambiar, M. P., Tsokos, G. C., and Farber, D. L. (2003) The FcRgamma subunit and Syk kinase replace the CD3zeta-chain and ZAP-70 kinase in the TCR signaling complex of human effector CD4 T cells, *J. Immunol. 170*, 4189−4195.
8. Call, M. E., Pyrdol, J., Wiedmann, M., and Wucherpfennig, K. W. (2002) The organizing principle in the formation of the T cell receptor-CD3 complex, *Cell 111*, 967−979.
9. Reth, M. (1989) Antigen receptor tail clue, *Nature 338*, 383−384.
10. Weiss, A. (1993) T cell antigen receptor signal transduction: a tale of tails and cytoplasmic protein-tyrosine kinases, *Cell 73*, 209−212.
11. Rudd, C. E. (1999) Adaptors and molecular scaffolds in immune cell signaling, *Cell 96*, 5−8.
12. van Oers, N. S., Love, P. E., Shores, E. W., and Weiss, A. (1998) Regulation of TCR signal transduction in murine thymocytes by multiple TCR zeta-chain signaling motifs, *J. Immunol. 160*, 163−170.
13. van Oers, N. S., Tohlen, B., Malissen, B., Moomaw, C. R., Afendis, S., and Slaughter, C. A. (2000) The 21- and 23-kD forms of TCR zeta are generated by specific ITAM phosphorylations, *Nat. Immunol. 1*, 322−328.
14. Futterer, K., Wong, J., Grucza, R. A., Chan, A. C., and Waksman, G. (1998) Structural basis for Syk tyrosine kinase ubiquity in signal transduction pathways revealed by the crystal structure of its regulatory SH2 domains bound to a dually phosphorylated ITAM peptide, *J. Mol. Biol. 281*, 523−537.
15. Folmer, R. H., Geschwindner, S., and Xue, Y. (2002) Crystal structure and NMR studies of the apo SH2 domains of ZAP-70: two bikes rather than a tandem, *Biochemistry 41*, 14176−14184.
16. Samelson, L. E. (2002) Signal transduction mediated by the T cell antigen receptor: the role of adapter proteins, *Annu. Rev. Immunol. 20*, 371−394.
17. Fahmy, T. M., Bieler, J. G., and Schneck, J. P. (2002) Probing T cell membrane organization using dimeric MHC−Ig complexes, *J. Immunol. Methods 268*, 93−106.
18. Reich, Z., Boniface, J. J., Lyons, D. S., Borochov, N., Wachtel, E. J., and Davis, M. M. (1997) Ligand-specific oligomerization of T-cell receptor molecule, *Nature 387*, 617−620.
19. Bachmann, M. F., and Ohashi, P. S. (1999) The role of T-cell receptor dimerization in T-cell activation, *Immunol. Today 20*, 568−576.
20. Cheng, P. C., Brown, B. K., Song, W., and Pierce, S. K. (2001) Translocation of the B cell antigen receptor into lipid rafts reveals a novel step in signaling, *J. Immunol. 166*, 3693−3701.
21. Ortega, E., Schweitzer-Stenner, R., and Pecht, I. (1988) Possible orientational constraints determine secretory signals induced by aggregation of IgE receptors on mast cells, *EMBO J. 7*, 4101−4109.
22. Ortega, E., Schweitzer-Stenner, R., and Pecht, I. (1991) Kinetics of ligand binding to the type 1 Fc epsilon receptor on mast cells, *Biochemistry 30*, 3473−3483.
23. Schweitzer-Stenner, R., Tamir, I., and Pecht, I. (1997) Analysis of Fc(epsilon)RI-mediated mast cell stimulation by surface-carried antigens, *Biophys. J. 72*, 2470−2478.
24. Tamir, I., and Cambier, J. C. (1998) Antigen receptor signaling: integration of protein tyrosine kinase functions, *Oncogene 17*, 1353−1364.
25. Holowka, D., and Baird, B. (1996) Antigen-mediated IGE receptor aggregation and signaling: a window on cell surface structure and dynamics, *Annu. Rev. Biophys. Biomol. Struct. 25*, 79−112.
26. Metzger, H. (1992) Transmembrane signaling: the joy of aggregation, *J. Immunol. 149*, 1477−1487.
27. Boniface, J. J., Rabinowitz, J. D., Wulfing, C., Hampl, J., Reich, Z., Altman, J. D., Kantor, R. M., Beeson, C., McConnell, H. M., and Davis, M. M. (1998) Initiation of signal transduction through the T cell receptor requires the multivalent engagement of peptide/MHC ligands [corrected], *Immunity 9*, 459−466.
28. Dintzis, R. Z., Okajima, M., Middleton, M. H., Greene, G., and Dintzis, H. M. (1989) The immunogenicity of soluble haptenated polymers is determined by molecular mass and hapten valence, *J. Immunol. 143*, 1239−1244.
29. Stone, J. D., Cochran, J. R., and Stern, L. J. (2001) T-cell activation by soluble MHC oligomers can be described by a two-parameter binding model, *Biophys. J. 81*, 2547−2557.
30. Thyagarajan, R., Arunkumar, N., and Song, W. (2003) Polyvalent antigens stabilize B cell antigen receptor surface signaling microdomains, *J. Immunol. 170*, 6099−6106.
31. Maurer, D., Fiebiger, E., Reininger, B., Ebner, C., Petzelbauer, P., Shi, G. P., Chapman, H. A., and Stingl, G. (1998) Fc epsilon receptor I on dendritic cells delivers IgE-bound multivalent antigens into a cathepsin S-dependent pathway of MHC class II presentation, *J. Immunol. 161*, 2731−2739.
32. Davis, M. M. (2002) A new trigger for T cells, *Cell 110*, 285−287.
33. Gil, D., Schamel, W. W., Montoya, M., Sanchez-Madrid, F., and Alarcon, B. (2002) Recruitment of Nck by CD3 epsilon reveals a ligand-induced conformational change essential for T cell receptor signaling and synapse formation, *Cell 109*, 901−912.
34. Reth, M., Wienands, J., and Schamel, W. W. (2000) An unsolved problem of the clonal selection theory and the model of an oligomeric B-cell antigen receptor, *Immunol. Rev. 176*, 10−18.
35. Kjer-Nielsen, L., Clements, C. S., Brooks, A. G., Purcell, A. W., McCluskey, J., and Rossjohn, J. (2002) The 1.5 Å crystal structure of a highly selected antiviral T cell receptor provides evidence for a structural basis of immunodominance, *Structure (Cambridge) 10*, 1521−1532.
36. Stewart-Jones, G. B., McMichael, A. J., Bell, J. I., Stuart, D. I., and Jones, E. Y. (2003) A structural basis for immunodominant human T cell receptor recognition, *Nat. Immunol. 4*, 657−663.
37. Garman, S. C., Kinet, J. P., and Jardetzky, T. S. (1998) Crystal structure of the human high-affinity IgE receptor, *Cell 95*, 951−961.
38. Garman, S. C., Wurzburg, B. A., Tarchevskaya, S. S., Kinet, J. P., and Jardetzky, T. S. (2000) Structure of the Fc fragment of human IgE bound to its high-affinity receptor Fc epsilonRI alpha, *Nature 406*, 259−266.
39. Garcia, K. C., Tallquist, M. D., Pease, L. R., Brunmark, A., Scott, C. A., Degano, M., Stura, E. A., Peterson, P. A., Wilson, I. A., and Teyton, L. (1997) Alphabeta T cell receptor interactions with syngeneic and allogeneic ligands: affinity measurements and crystallization, *Proc. Natl. Acad. Sci. U.S.A. 94*, 13838−13843.
40. Weissenhorn, W., Eck, M. J., Harrison, S. C., and Wiley, D. C. (1996) Phosphorylated T cell receptor zeta-chain and ZAP70 tandem SH2 domains form a 1:3 complex in vitro, *Eur. J. Biochem. 238*, 440−445.
41. Borroto, A., Jimenez, M. A., Alarcon, B., and Rico, M. (1997) 1H NMR analysis of CD3-epsilon reveals the presence of turn-helix structures around the ITAM motif in an otherwise random coil cytoplasmic tail, *Biopolymers 42*, 75−88.
42. Laczko, I., Hollosi, M., Vass, E., Hegedus, Z., Monostori, E., and Toth, G. K. (1998) Conformational effect of phosphorylation on T cell receptor/CD3 zeta-chain sequences, *Biochem. Biophys. Res. Commun. 242*, 474−479.
43. Klemm, J. D., Schreiber, S. L., and Crabtree, G. R. (1998) Dimerization as a regulatory mechanism in signal transduction, *Annu. Rev. Immunol. 16*, 569−592.

44. Iakoucheva, L. M., Brown, C. J., Lawson, J. D., Obradovic, Z., and Dunker, A. K. (2002) Intrinsic disorder in cell-signaling and cancer-associated proteins, *J. Mol. Biol. 323*, 573−584.
45. Uversky, V. N., Gillespie, J. R., and Fink, A. L. (2000) Why are "natively unfolded" proteins unstructured under physiologic conditions?, *Proteins 41*, 415−427.
46. Dunker, A. K., Brown, C. J., Lawson, J. D., Iakoucheva, L. M., and Obradovic, Z. (2002) Intrinsic disorder and protein function, *Biochemistry 41*, 6573−6582.
47. Dunker, A. K., Brown, C. J., and Obradovic, Z. (2002) Identification and functions of usefully disordered proteins, *Adv. Protein Chem. 62*, 25−49.
48. Tompa, P. (2002) Intrinsically unstructured proteins, *Trends Biochem. Sci. 27*, 527−533.
49. Aivazian, D., and Stern, L. J. (2000) Phosphorylation of T cell receptor zeta is regulated by a lipid dependent folding transition, *Nat. Struct. Biol. 7*, 1023−1026.
50. Kratochvil, P. (1987) *Classical Light Scattering from Polymer Solutions*, Elsevier Science Publishers B.V., Amsterdam.
51. McRorie, D. K., and Voelker, P. J. (1993) *Self-Associating Systems in the Analytical Ultracentrifuge*, Vol. II, Beckman Instruments, Palo Alto, CA.
52. Bax, A., Ikura, M., Kay, L. E., Torchia, D. A., and Tschudin, R. (1990) Comparison of different modes of 2D reverse correlation NMR for the study of proteins, *J. Magn. Reson. 86*, 304−318.
53. Kuzmic, P. (1998) Fixed-point methods for computing the equilibrium composition of complex biochemical mixtures, *Biochem. J. 331* (Part 2), 571−575.
54. Dyson, H. J., and Wright, P. E. (1998) Equilibrium NMR studies of unfolded and partially folded proteins, *Nat. Struct. Biol. 5* (Suppl.), 499−503.
55. Dyson, H. J., and Wright, P. E. (2002) Insights into the structure and dynamics of unfolded proteins from nuclear magnetic resonance, *Adv. Protein Chem. 62*, 311−340.
56. Eliezer, D., Yao, J., Dyson, H. J., and Wright, P. E. (1998) Structural and dynamic characterization of partially folded states of apomyoglobin and implications for protein folding, *Nat. Struct. Biol. 5*, 148−155.
57. Zhang, O., Forman-Kay, J. D., Shortle, D., and Kay, L. E. (1997) Triple-resonance NOESY-based experiments with improved spectral resolution: applications to structural characterization of unfolded, partially folded and folded proteins, *J. Biomol. NMR 9*, 181−200.
58. Clark, M. R., Campbell, K. S., Kazlauskas, A., Johnson, S. A., Hertz, M., Potter, T. A., Pleiman, C., and Cambier, J. C. (1992) The B cell antigen receptor complex: association of Ig-alpha and Ig-beta with distinct cytoplasmic effectors, *Science 258*, 123−126.
59. Sanchez, M., Misulovin, Z., Burkhardt, A. L., Mahajan, S., Costa, T., Franke, R., Bolen, J. B., and Nussenzweig, M. (1993) Signal transduction by immunoglobulin is mediated through Ig alpha and Ig beta, *J. Exp. Med. 178*, 1049−1055.
60. Kim, K. M., Alber, G., Weiser, P., and Reth, M. (1993) Differential signaling through the Ig-alpha and Ig-beta components of the B cell antigen receptor, *Eur. J. Immunol. 23*, 911−916.
61. Xu, W., Harrison, S. C., and Eck, M. J. (1997) Three-dimensional structure of the tyrosine kinase c-Src, *Nature 385*, 595−602.
62. Housden, H. R., Skipp, P. J., Crump, M. P., Broadbridge, R. J., Crabbe, T., Perry, M. J., and Gore, M. G. (2003) Investigation of the kinetics and order of tyrosine phosphorylation in the T-cell receptor zeta chain by the protein tyrosine kinase Lck, *Eur. J. Biochem. 270*, 2369−2376.
63. Borroto, A., Mallabiabarrena, A., Albar, J. P., Martinez, A. C., and Alarcon, B. (1998) Characterization of the region involved in CD3 pairwise interactions within the T cell receptor complex, *J. Biol. Chem. 273*, 12807−12816.
64. Torres, J., Briggs, J. A., and Arkin, I. T. (2002) Multiple site-specific infrared dichroism of CD3-zeta, a transmembrane helix bundle, *J. Mol. Biol. 316*, 365−374.
65. Torres, J., Briggs, J. A., and Arkin, I. T. (2002) Convergence of experimental, computational and evolutionary approaches predicts the presence of a tetrameric form for CD3-zeta, *J. Mol. Biol. 316*, 375−384.
66. Spencer, D. M., Wandless, T. J., Schreiber, S. L., and Crabtree, G. R. (1993) Controlling signal transduction with synthetic ligands, *Science 262*, 1019−1024.
67. Soldevila, G., Castellanos, C., Malissen, M., and Berg, L. J. (2001) Analysis of the individual role of the TCRzeta chain in transgenic mice after conditional activation with chemical inducers of dimerization, *Cell Immunol. 214*, 123−138.
68. Crabtree, G. R., and Schreiber, S. L. (1996) Three-part inventions: intracellular signaling and induced proximity, *Trends Biochem. Sci. 21*, 418−422.
69. Watowich, S. S., Liu, K. D., Xie, X., Lai, S. Y., Mikami, A., Longmore, G. D., and Goldsmith, M. A. (1999) Oligomerization and scaffolding functions of the erythropoietin receptor cytoplasmic tail, *J. Biol. Chem. 274*, 5415−5421.
70. Li, R., Babu, C. R., Lear, J. D., Wand, A. J., Bennett, J. S., and DeGrado, W. F. (2001) Oligomerization of the integrin alphaIIbbeta3: roles of the transmembrane and cytoplasmic domains, *Proc. Natl. Acad. Sci. U.S.A. 98*, 12462−12467.
71. Johansson, B., Palmer, E., and Bolliger, L. (1999) The extracellular domain of the zeta-chain is essential for TCR function, *J. Immunol. 162*, 878−885.
72. Rutledge, T., Cosson, P., Manolios, N., Bonifacino, J. S., and Klausner, R. D. (1992) Transmembrane helical interactions: zeta chain dimerization and functional association with the T cell antigen receptor, *EMBO J. 11*, 3245−3254.
73. Kishimoto, H., Kubo, R. T., Yorifuji, H., Nakayama, T., Asano, Y., and Tada, T. (1995) Physical dissociation of the TCR−CD3 complex accompanies receptor ligation, *J. Exp. Med. 182*, 1997−2006.
74. Liu, H., Rhodes, M., Wiest, D. L., and Vignali, D. A. (2000) On the dynamics of TCR:CD3 complex cell surface expression and downmodulation, *Immunity 13*, 665−675.
75. Kosugi, A., Saitoh, S., Noda, S., Yasuda, K., Hayashi, F., Ogata, M., and Hamaoka, T. (1999) Translocation of tyrosine-phosphorylated TCRzeta chain to glycolipid-enriched membrane domains upon T cell activation, *Int. Immunol. 11*, 1395−1401.
76. Ono, S., Ohno, H., and Saito, T. (1995) Rapid turnover of the CD3 zeta chain independent of the TCR−CD3 complex in normal T cells, *Immunity 2*, 639−644.
77. Vilen, B. J., Nakamura, T., and Cambier, J. C. (1999) Antigen-stimulated dissociation of BCR mIg from Ig-alpha/Ig-beta: implications for receptor desensitization, *Immunity 10*, 239−248.
78. Asai, K., Fujimoto, K., Harazaki, M., Kusunoki, T., Korematsu, S., Ide, C., Ra, C., and Hosoi, S. (2000) Distinct aggregation of beta- and gamma-chains of the high-affinity IgE receptor on cross-linking, *J. Histochem. Cytochem. 48*, 1705−1716.

BI035900H